



ELSEVIER

Available online at [www.sciencedirect.com](http://www.sciencedirect.com)**ScienceDirect**[www.elsevier.com/locate/jmbbm](http://www.elsevier.com/locate/jmbbm)**Research paper****Nacre-like materials using a simple doctor blading technique: Fabrication, testing and modeling****M. Mirkhala<sup>f</sup>, F. Barthelat<sup>\*</sup>**

Department of Mechanical Engineering, McGill University, 817 Sherbrooke Street West, Montreal, Quebec, Canada H3A 2K6

**ARTICLE INFO****Article history:**

Received 7 May 2015

Received in revised form

7 November 2015

Accepted 16 November 2015

Available online 1 December 2015

**Keywords:**

Artificial nacre

Bio-inspired materials

Staggered composites

Optimization

Finite element modeling

**ABSTRACT**

The remarkable mechanical performance of biological materials such as bone, nacre, and spider silk stems from their staggered microstructure in which stiff and strong reinforcements are elongated in the direction of loading, separated by softer interfaces, and shifted relative to each other. This structure results in useful combinations of modulus, strength and toughness and therefore is increasingly mimicked in bio-inspired engineering composites. Here, we report the use of a simple and versatile technique based on doctor-blading to fabricate staggered composites of microscopic alumina tablets with high alignment in a chitosan matrix. Tensile tests on these nacre-like materials show that the modulus and strength of the composite films are enhanced by the incorporation of ceramic tablets, but only up to 15 vol% after which all properties degrade. This phenomenon, also reported in the past for most of nacre-like materials, composed of micro/nano tablets, obtained from different techniques, has been limiting our ability to produce large volumes of high-performance nacre-like materials. Examination of the structure of the films revealed that at lower tablet concentrations the tablets are well-aligned and well dispersed thorough the volume of the film. At 15 vol% and beyond, we observed tablet misalignment and clustering. In order to investigate the impact of these imperfections on material performance we developed large scale finite element models representative of the structure of the composite films. These models show that the mechanical performance significantly degrades with tablet misalignment, and especially at high tablet concentrations. The simulations along with the SEM images therefore quantitatively explain the experimental trends, e.g. the degradation of mechanical properties at high tablet contents.

© 2015 Elsevier Ltd. All rights reserved.

**1. Introduction**

Natural materials such as bone (Jager and Fratzl, 2000), nacre (Jackson et al., 1988), tooth enamel (Gao et al., 2003), and spider silk (Buehler et al., 2008) boast unusual and attractive combinations of properties which surpass their engineering

counterparts (Ashby et al., 1995; Barthelat, 2007). In particular, these materials combine high strength and high toughness (energy absorption), two properties which are very difficult to achieve simultaneously in engineering materials (Ritchie, 2011). A general strategy which is pervasive across these high-performance materials is the combination of very

\*Corresponding author.

E-mail address: [francois.barthelat@mcgill.ca](mailto:francois.barthelat@mcgill.ca) (F. Barthelat).

hard and very soft components arranged in complex hierarchical architectures (Meyers et al., 2008; Wise, 1970). A key microstructure across these materials is the staggered arrangement, where stiff and elongated inclusions are aligned with some degree of overlap within a softer matrix (Barthelat, 2007; Barthelat et al., 2007; Currey and Taylor, 1974; Fratzl, 2003; Mirkhalaf et al., 2013). Recent studies revealed that the staggered microstructure is optimum when modulus, strength and toughness are simultaneously desired (Barthelat and Mirkhalaf, 2013; Guo and Gao, 2006). Mollusk species such as *Pinctada* or *Pinna nobilis* have nacreous shells with typical staggered microstructures. Sheet nacre from *Pinctada* is typically composed of ~95 wt% microscopic aragonite tablets which are arranged in a highly regular staggered structure and bonded by ~5 wt% soft polymers which are commonly called “interfaces”. The mechanisms of deformation and fracture associated with this microstructure provides interesting combinations of mechanical properties (Barthelat, 2014; Currey, 1977; Jackson et al., 1988; Katti et al., 2001; Wang et al., 2001). In particular, sheet nacre from *Pinctada* is almost as stiff as aragonite yet it is ~3000 times tougher (Fig. 1a) which is a remarkable level of “toughness amplification” by any standard (Jackson et al., 1988; Rabiei et al., 2010). Several mechanisms including crack bridging, deflection and process zone contribute to this outstanding toughness amplification (Fig. 1b) (Barthelat and Rabiei, 2011; Ortiz and Boyce, 2008). These remarkable mechanics and properties of natural staggered composites and in particular of sheet nacre from *Pinctada* has motivated the development and fabrication of a large variety of nacre-like synthetic materials over the past two decades. A wide variety of methods were proposed to fabricate nacre-like structures: sputtering (He et al., 1997), centrifugation and casting (Almqvist et al., 1999), layer by layer assembly (Podsiadlo et al., 2007; Tang et al., 2003), freeze casting of inorganic layers followed by a polymer or a metal filling stage (Deville et al., 2006; Munch et al., 2008), sequential Langmuir–Blodgett film/polymer deposition (Bonderer et al., 2008), vacuum filtration (Yao et al., 2010), sedimentation (Walther et al., 2010), ink-jet printing (Andres and Kotov, 2010), and freeze casting of micro-tablets (Bouville et al., 2014; Hunger et al., 2012) have been utilized to develop bio-inspired staggered composites at micro/nano-scales. In order to have a better control over the morphology of the material, staggered

structures have also been fabricated at larger length scales using variety of methods including manual assembly of flat (Clegg et al., 1990; Mayer, 2006) and wavy tablets (Barthelat and Zhu, 2011), rapid prototyping (Espinosa et al., 2009), 3D printing (Dimas et al., 2013), and laser engraving (Mirkhalaf and Barthelat, 2015; Mirkhalaf et al., 2014).

Many of these materials display interesting combinations of mechanical properties (Bonderer et al., 2008; Munch et al., 2008), but the level of toughness amplification and structural organization achieved in these materials is still inferior compared to those of natural nacre. Some of the fabrication methods proposed can also only be used for small volumes of material and cannot scale up to production scales. The most efficient method to make nacre-like materials easily and on large scale remains to this day the “mixing” method, where flat ceramic or mineral platelets are mixed in a solvated polymer, and subsequently aligned using mechanical stress (Almqvist et al., 1999), sedimentation (Walther et al., 2010) or magnetic fields (Erb et al., 2012). A possible limitation of these approaches is that it is difficult to achieve high concentrations of tablets because of the limited packing efficiency. Arrangement and packing of the tablets can be improved using self-assembly (Mirkhalaf et al., 2015), but this careful process is more time consuming and can so far only be performed layer by layer. For all these nacre-like materials, increases of stiffness and strength were reported, but only up to tablet concentrations of 10–20%. This comparably low tablet content results in microstructural characteristics which are far from nacre. However, these materials possess interesting properties rooted in their staggered structure which has been numerically found to be optimum even at low tablet contents when a combination of mechanical properties is desired (Mirkhalaf and Barthelat, 2014). Beyond the 10–20 vol% tablet content threshold, all the mechanical properties of these materials decrease down to levels which may be even lower than the properties of the pure matrix (Bonderer et al., 2008; Das et al., 2013; Podsiadlo et al., 2007). This experimental result, contradicts the prediction of models which suggest that very large concentration of tablets should lead to very high modulus and strength (Jager and Fratzl, 2000). In natural nacre, which serves as model for these bio-inspired composites, the concentration of the mineral tablets is as high as 95 wt%. The fact that synthetic nacres only achieve high properties up to 10–20 vol%

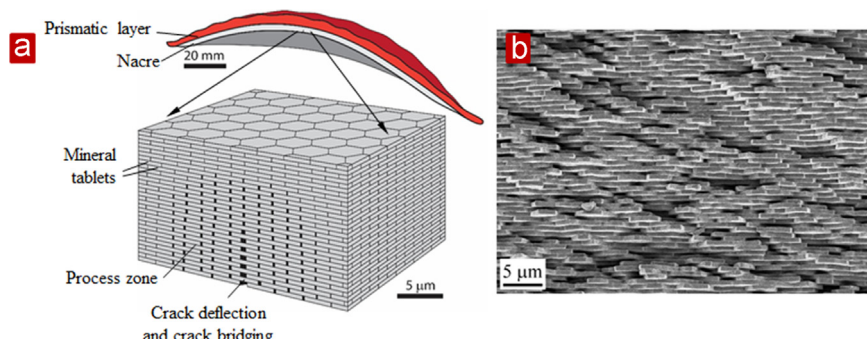


**Fig. 1 – (a) Schematic of the microstructure of nacre showing the deformation and toughening mechanisms, (b) SEM image of a fracture surface of a *Pinctada* nacre showing the staggered arrangement of tablets.**

concentration of tablets indicates serious limitations which could be associated with poor alignment of the tablets and/or poor dispersion and clustering of inclusions, a well-known issue in carbon nanotube-reinforced polymers (Qian et al., 2010). This discrepancy, reported in several experimental studies on staggered composites (Bonderer et al., 2008; Das et al., 2013; Podsiadlo et al., 2007), is not fully understood to this day. Only a few experimental studies examined the effect of imperfections within the microstructure on the degradation of the mechanical properties at high tablet concentrations (Wang et al., 2013). In this article we characterize the structure and properties of nacre-like films of micron-sized alumina tablets embedded in a chitosan matrix. The films are fabricated using a doctor-blading method, which is relatively simple and scalable. We report the mechanical properties of this film as function of tablet concentration, and we then present finite element models which capture possible limitations of mechanical improvements due to imperfections in the microstructure.

## 2. Preparation and characterization of nacre-like alumina-chitosan thin films

The fabrication of the composite material started with a 0.1 molar (with respect to monomer) solution of chitosan (Sigma Aldrich, MO, US) prepared in a 2 wt% solution of acetic acid (Sigma Aldrich, MO, US) in water. Microscopic alumina tablets (Antaria limited, WA, Australia) were used as reinforcing inclusions. The tablets have a diameter of  $10.5 \pm 3.2 \mu\text{m}$  and thickness of  $0.41 \pm 0.11 \mu\text{m}$  (Fig. 2a), which was characterized using scanning electron microscopy on four samples. Before mixing, the tablets were functionalized with a 3-aminopropyltriethoxysilane (APTS) coating, following Bonderer et al. (2008). Silane functionalization of the surfaces of the ceramic tablets improves the polymer-

particle bonding and results in a higher composite modulus and strength (Guo et al., 2006; Ma et al., 2007). A controlled amount of the coated platelets was then mixed with 10 mL of chitosan solution, which resulted in a milky slurry. This slurry was ultrasonicated for 10 min in order to disperse the ceramic tablets, and stirred under constant air flow for one day in order to accelerate the evaporation of the water and of the acetic acid. This process yielded a  $\sim 2 \text{ ml}$  viscous paste, which was then doctor bladed with a spatula on an acrylic substrate (Fig. 2b). Following doctor blading the film was dried for 24 h at room temperature, while the shrinkage associated with drying released the film from the acrylic substrate (Fig. 2c). Films with increasing tablet concentration ( $\phi = 0, 5, 10, 15, 20, 50$  and 80 vol%) were produced using this method. The films had a decreasing transparency and slightly increased thickness as the volume concentration of alumina tablets was increased (Fig. 2d). The film thickness was  $\sim 20 \mu\text{m}$  for the composites with the lowest ceramic content ( $\phi = 5 \text{ vol\%}$ ) and increased with the ceramic content to  $\sim 30 \mu\text{m}$  for the material with  $\phi = 80 \text{ vol\%}$ .

The initial thickness of the paste after doctor blading was the same ( $\sim 120 \mu\text{m}$ ) for the samples with different tablet contents. However, after the water and acid acetic which were used to dissolve the polymer evaporated, the thickness reduced. This reduction was more pronounced for the materials with higher polymer and lower tablet content and as a result these films were thinner compared to the films with higher tablet contents. Examination of the microstructure of these films revealed a high degree of alignment between the ceramic tablets resulting in a nacre-like micro-architecture. Fig. 3a shows the arrangement of tablets within a fracture surface image of a composite film with 10% tablet content. The tablets are shown with red-bordered boxes in order to better reveal their arrangement. The results show that the tablets are not necessarily arranged in distinct multiple layers or

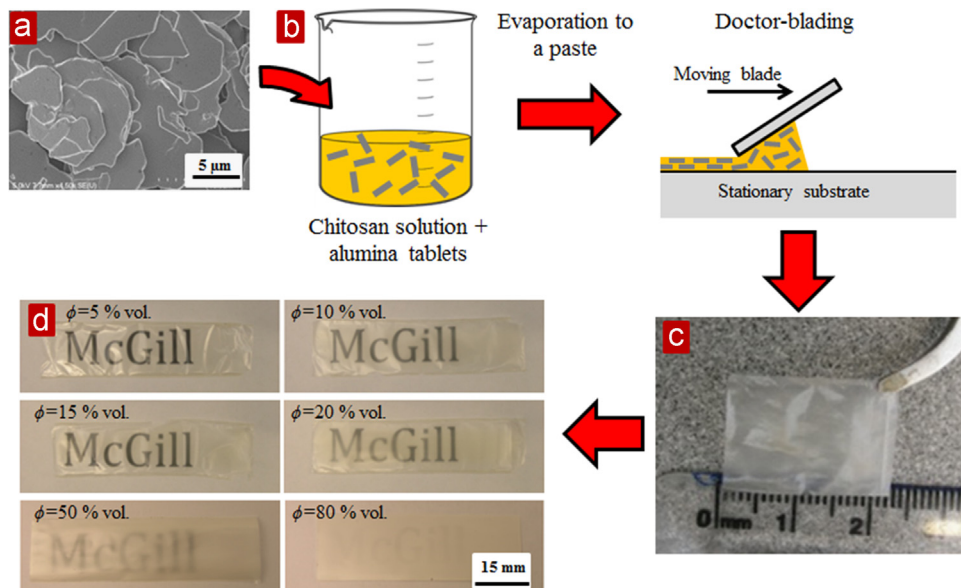


**Fig. 2 – (a)** A SEM image of alumina tablets, showing their size and shape, **(b)** schematic of the fabrication process, **(c)** optical image of the film with 15 vol% tablet concentration released from the substrate **(d)** optical images of the composite films with 5, 10, 15, 20, 50 and 80 vol% ceramic concentrations ( $\phi$  denotes the tablet volume concentration).

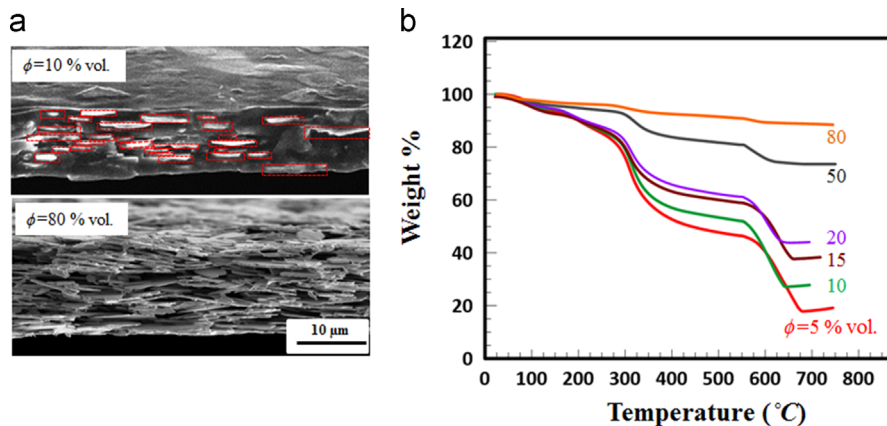


**Fig. 3 – (a)** Secondary electron mode SEM images of the fracture surface of the doctor-bladed alumina/chitosan composite films with 10 vol%, and 80 vol% tablet concentrations, showing the staggered arrangement of the tablets. The fracture surfaces are coated with a 20 nm layer of gold–platinum, **(b)** TGA analysis results of the  $\text{Al}_2\text{O}_3/\text{chitosan}$  composite films with different tablet concentrations ( $\phi$  denotes the tablet volume concentration).

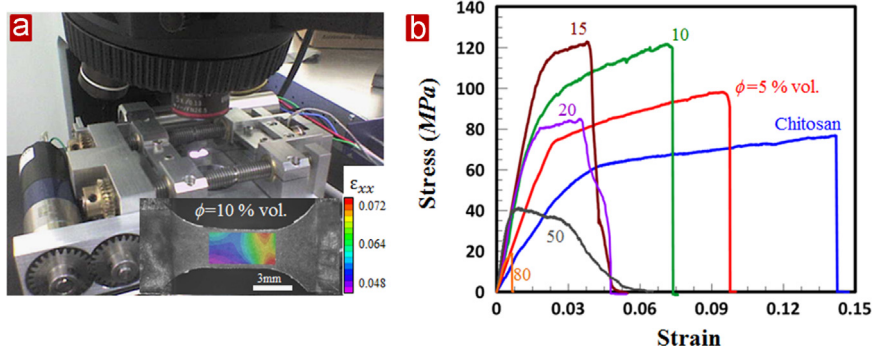


**Fig. 4 – (a)** The loading set up for the tensile tests. The distribution of the tensile strain for a dogbone sample with 10 vol% tablet concentration at an average tensile strain of 0.06, **(b)** tensile stress–strain curves of the composite films with different tablet concentrations.

columns. However, they are aligned to each other in a 3D structure and arranged in a staggered structure which is a key to the mechanical performance of the composite films. The results confirm that doctor blading can not only be used to control the thickness of the film, but also to align the micro-tablets within the matrix in a manner similar to the extrusion of short fiber reinforced composites (Barbosa and Kenny, 2000; Joseph et al., 1993). The tablet concentration in the composite films was confirmed with Thermo-Gravimetric Analysis (TGA). For each tablet concentration, TGA analysis was performed on 3–6 mg of the composite film with the heating rate of 20 °C/min using a Q500 thermogravimetric analyzer (TA instruments, USA). The samples were heated up to 550 °C in a nitrogen medium and then up to 750 °C in an air medium. 5% weight loss was found for temperatures below 100 °C corresponding to the evaporation of water and acetic acid. Chitosan chains were mostly thermally decomposed at higher temperatures (300–350 °C). The remaining carbon was then oxidized by changing the carrier gas to oxygen at 550 °C. Only ceramic tablets remained at 750 °C. The results confirmed the expected tablet concentration in the composites (Fig. 3b).

### 3. Mechanical performance

Dog-bone samples with a  $3 \times 5 \text{ mm}^2$  gage area were cut from the film using a pulsed laser (Model Vitrolux, Vitro Laser Solutions UG, Minden, Germany), and were tested in tension using a miniature loading stage (Ernest F. Fullam, Latham, NY) under an optical upright microscope (BX-51M, Olympus, Markham, Canada). All tests were performed at a quasi-static strain rate of  $5 \times 10^{-4}/\text{s}$ , and at a controlled humidity of 30–35%. In-situ images acquired during the tensile tests were used to measure the full strain fields at different points during the experiment, using Digital Image Correlation (DIC) (VIC-2D, Correlated Solutions, SC, USA, Fig. 4a). The natural texture of the film was sufficient to serve as random speckle to perform digital image correlations. The inset of Fig. 4a shows a typical strain field for films with low tablet concentrations ( $\phi = 10 \text{ vol\%}$ ) at an average tensile strain of 0.06. For these low-concentrations the tensile strain in the film was relatively uniform in the gage area of the samples, until localization occurred just before failure. For the samples with higher tablet concentrations ( $20 \leq \phi < 80 \text{ vol\%}$ ), the strain localization and cracks appeared at relatively earlier stages

of the loading (e.g. at 1% tensile strain for the film with 50 vol% tablets). A crack then propagated slowly across the sample until the material completely failed. At very high tablet concentration ( $\phi \approx 80$  vol%), the material failed in a brittle fashion at small deformations (strain  $< 0.7\%$ ). Fig. 4b shows a set of typical tensile stress–strain curves for different tablet concentrations (with strains measured from digital image correlation). Pure chitosan showed an initial linear elastic region (modulus =  $1.88 \pm 0.12$  GPa) followed by a yield point at about 60 Mpa and inelastic deformations with hardening. At about 14% tensile strain and at ultimate tensile strength of about 72.5 Mpa, the film rapidly fractured. The incorporation of ceramic tablets up to 15 vol% did not alter the overall shape of the curve but resulted in increased modulus and strength, at the expense of ductility and energy absorption (area under the stress–strain curve). The 15 vol% film had a modulus of  $7 \pm 1.2$  Gpa (which is about four times stiffer than the pure chitosan), a strength of about 120 Mpa (about double that of pure chitosan), and energy absorption of  $4.3 \text{ MJ m}^{-3}$  (about half of that of pure chitosan). Bonderer et al. (2008) reported similar composite films made by layer by layer (LBL) assembly of alumina tablets and chitosan. They also observed a peak in the mechanical properties of the films at 15 vol% tablet concentration. Their film had a modulus of  $9.6 \pm 2$  Gpa (~4 times that of the utilized chitosan) and the strength of 300 Mpa (~6 times that of the utilized chitosan). The modulus, yield strength and the strain at failure of the chitosan utilized in Bonderer et al. are  $\sim 2.4$  Gpa,  $\sim 50$  Mpa and  $\sim 0.35$  respectively. That chitosan was therefore more deformable, stiffer and slightly weaker compared to the chitosan we used in this study. The range of modulus and the level of its improvement over chitosan, obtained in Bonderer et al., are in the same order as we have achieved using the inexpensive, fast and versatile doctor blading technique. However, in terms of strength, Bonderer et al. amplified the strength of chitosan by a factor of  $\sim 6$  while we achieved an improvement by a factor of  $\sim 2$ . This higher performance might be largely due to the higher aspect ratio of the alumina tablets utilized in Bonderer et al. ( $\rho \approx 40$ ), compared to what we found for the alumina tablet utilized in this study ( $\rho \approx 25$ ). Using higher aspect ratio alumina tables in the doctor-blading process can therefore yield composites with higher strength (Glavinchevski and Piggott, 1973). The doctor blading technique is also more versatile, much faster and easier to implement compared to the LBL technique.

Fig. 5 summarizes how the modulus, strength and energy absorption (normalized by the properties of pure chitosan) evolve with tablet concentration. As expected, the energy absorption decreases when the tablet concentration is increased. For the films with tablet concentrations higher than 15 vol%, all mechanical properties degraded (Fig. 4b). While this result is consistent with previous reports of experimental work on nano-composites (Qian et al., 2010) and nacre-like materials (Bonderer et al., 2008; Das et al., 2013; Podsiadlo et al., 2007), the trend contradicts the existing models and predictions for staggered composites which predict higher strength and stiffness for high mineral concentrations (Barthelat and Rabiei, 2011; Bekah et al., 2011; Kotha et al., 2001).

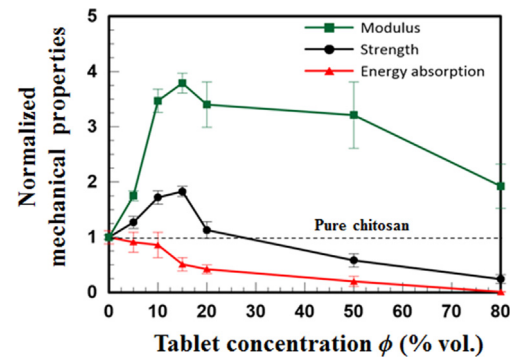
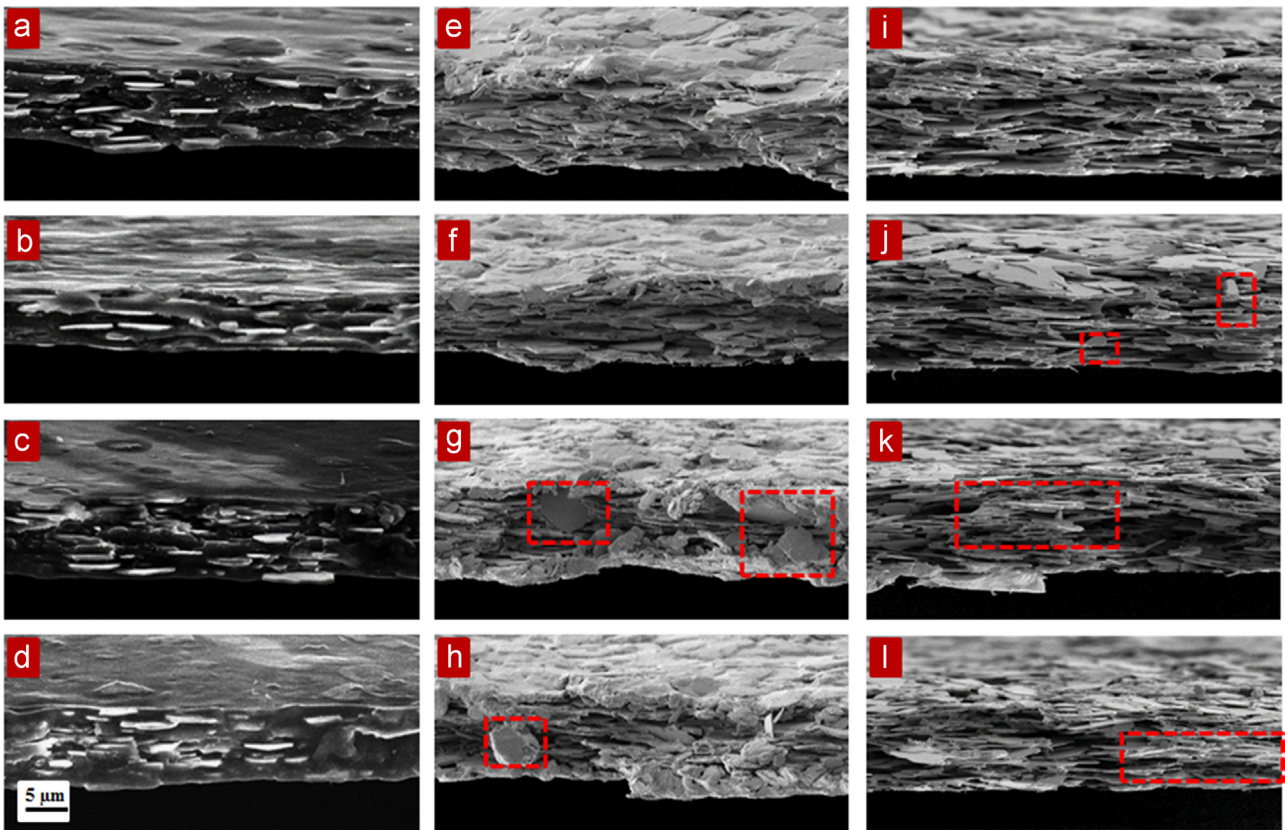


Fig. 5 – The normalized modulus, strength, and energy absorption of the composites with different tablet concentrations. The results show that all the mechanical properties degrade for tablet concentrations more than 15 vol%.

A likely explanation for this negative trend is that the arrangement of the tablets degrades as their volume fraction is increased. Fig. 6 shows the SEM micrographs of the fracture surfaces of the composites with three different tablet concentrations ( $\phi = 10, 50, 80$  vol%). At low tablets concentration (e.g.  $\phi = 10$  vol%, Fig. 6a–d) the tablets are well-aligned and uniformly distributed within the film. Micrographs of the fracture surface of the materials with higher tablet concentrations (e.g.  $\phi = 50$  vol%, Fig. 6e–h) also show relatively well-aligned and well dispersed tablets with no apparent clustering, but a few misaligned tablets (Fig. 6g and h) are also observed. These misaligned tablets are few but may act similar to penny cracks perpendicular to the direction of loading, possibly greatly reducing the tensile strength of the material. During the doctor-blading process of films with high tablet concentration, the tablets strongly interact, preventing their alignment with the shear flow of the matrix. In extreme cases, some tablets are confined by neighboring ones into completely misaligned orientations, with large impacts on the mechanical performance. In contrast, at lower tablet concentrations the tablets have more freedom to move and rotate within the polymer matrix to align with the shear flow of the matrix, reducing misalignment (Fig. 6g and h). At very high tablet concentrations ( $\phi = 80$  vol%, Fig. 6i–l) misaligned tablets were again observed, and in addition pores and clustering of tablets could also be seen. A possible reason is that the amount of polymer in the film (20 vol%) is not sufficient to infiltrate the open spaces and gaps between the tablets. As a result, the film containing high-concentration of tablets showed regions where the polymer phase is entirely absent (Fig. 6i–l). There are therefore several possible scenarios which can explain the low of strength at high tablet concentration. Some of these scenarios were explored using microstructure-level finite element simulations presented in the next section.

#### 4. Numerical simulations

In order to provide more insights into the structure–property relations in staggered composites and in order to address the



**Fig. 6 – SEM images of the fracture surfaces of the composite films with: (a–d) 10 vol% alumina showing the high level of alignment between the tablets, (e and f) 50 vol% alumina showing the well aligned nacre-like morphology of the material, (g and h) 50 vol% alumina showing the misaligned tablets, (i) 80 vol% alumina showing the nacre-like morphology of the material but with lots of empty spaces, (j) 80 vol% alumina showing the misaligned tablets, (k and l) 80 vol% alumina showing the tablet clustering and empty spaces.**

experimental trends namely the degradation of mechanical properties at high tablet concentrations, two-dimensional Representative Volume Elements (RVE) of the staggered microstructure at various tablet content and with various degrees of defects were developed. Large square shaped RVEs containing tablets at random positions were built using Matlab (R2012a, MA, US). A random sequential adsorption (RSA) algorithm (Rintoul and Torquato, 1997) was used to build the RVEs. In this approach tablets were created one by one and assigned to a random position within the volume of the RVE. The position of the tablet was confirmed if no collision was detected with other tablets already in the RVE, using a collision check algorithm. This process continued until the desired tablet concentration was reached. The angle of the tablets with respect to the loading direction  $\theta$  was selected based on a normal distribution centered on  $\theta=0$  and with a standard deviation  $\Delta\theta$ .  $\Delta\theta$  could be increased from zero (perfect alignment) to larger values to introduce statistical misalignment of the tablets. This RVE generation method resulted in arbitrary but statistically homogenous microstructures (Fig. 7). The RSA algorithm could generate RVEs with tablet concentration of only up to almost 50 vol%, after which the algorithm saturated and no additional tablets could be added without colliding the already existing tablets within the RVE. Since no size effect was considered in the model, the

thickness of the tablets was set to one and their length was fixed to 25 (therefore their aspect ratio was  $\rho=25$ , which is the actual average aspect ratio of the alumina tablets used in the experiments). The RVE was meshed with 8-node plane strain quadratic elements in ANSYS (version 9, PA, US). The mesh size was refined until the tensile behavior of the RVE did not alter with further mesh refinement. The tablets and matrix were assigned material properties corresponding to chitosan and alumina. Chitosan was modeled using a bilinear elastic-plastic model, with yielding behavior governed by the Von Mises criterion. The elasto-plastic properties of chitosan were obtained from the experimental stress-strain curves: elastic modulus  $E_0 = 1.88$  GPa and yield strength  $\sigma_y = 52$  MPa. The tangent modulus was obtained from the slope of the stress-strain curve in the post-yielding region ( $E_t = 115$  MPa). A Poisson's ratio of 0.4 was used for chitosan (a typical value for polymers). The alumina tablets were modeled as a linear elastic material (modulus  $E_m = 330$  GPa, Poisson's ratio  $\nu_m = 0.2$ ) (Knudsen, 1962). The fracture of the tablets was not included in the model, because from the experiments yielding of the matrix and pullout of the inclusions are the dominant failure modes. The two phases were assumed to be perfectly bonded. Displacement boundary conditions were applied to the edges of the RVE to enforce periodic boundary conditions along the two perpendicular x and y directions

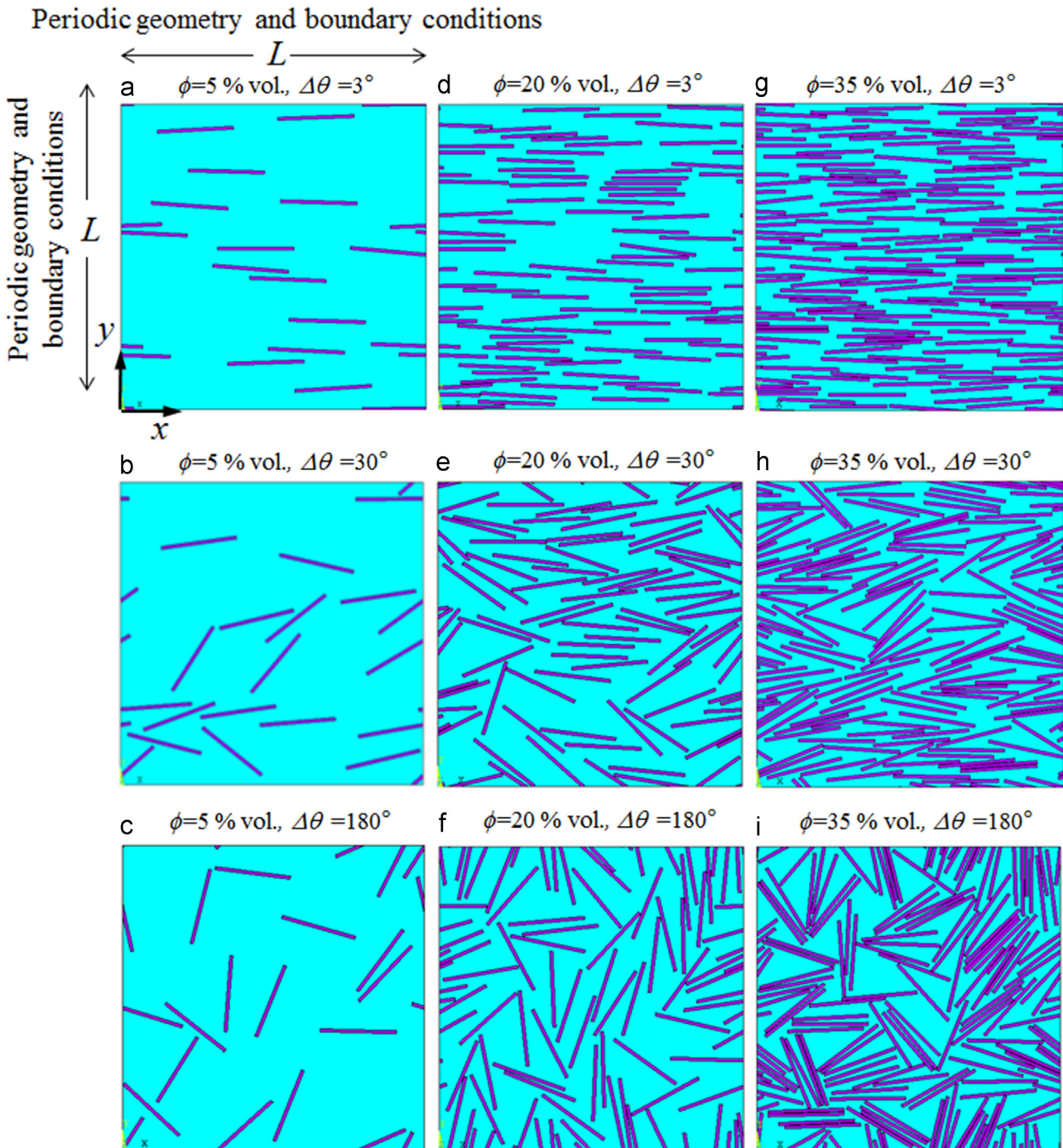


**Fig. 7 – RVEs for materials with a range of tablet contents and orientations:** (a, b, and c)  $\phi=5$  vol%, and  $\Delta\theta=3^\circ$ ,  $30^\circ$ , and  $180^\circ$ , respectively, (d, e, and f)  $\phi=20$  vol%, and  $\Delta\theta=3^\circ$ ,  $30^\circ$ , and  $180^\circ$  respectively (g, h, and i)  $\phi=35$  vol%, and  $\Delta\theta=3^\circ$ ,  $30^\circ$ , and  $180^\circ$  respectively.

(Eq. (1), Fig. 7a).

$$\left\{ \begin{array}{l} u_x(0,0) = u_y(0,0) = 0 \\ u_x(L,y) - u_x(0,y) = \bar{\epsilon}_{xx}L \\ u_y(L,y) = u_y(0,y) \\ u_y(x,L) - u_y(x,0) = \bar{\epsilon}_{yy}L \\ u_x(x,L) = u_x(x,0) \end{array} \right. \quad (1)$$

where  $u_x$  and  $u_y$  denote the horizontal and vertical displacements.

In order to apply the tensile deformation, the overall strain along the horizontal direction progressively increased by applying the constraints on the right/left boundary nodes (Eq. (1)). Fig. 8 shows typical distributions of first principal strain  $\epsilon_{\max}$  at different stages of loading. As the RVE was stretched horizontally, a network of deformation bands propagated throughout the model (Fig. 8a-d). In the simulations, we assumed that the matrix failed once one of these deformation bands with first principal strain ( $\epsilon_{\max}$ ) higher

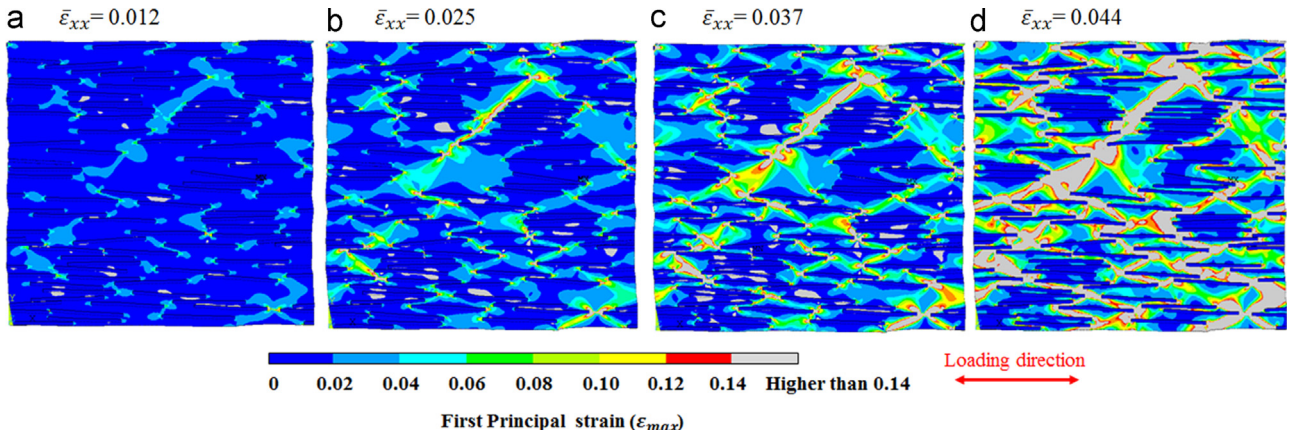


**Fig. 8 – distribution of first principal strain  $\epsilon_{\max}$  at different stages of loading for an example RVE with 20 vol% tablet concentration, (a) at average tensile strain of  $\bar{\epsilon}_{xx} = 0.012$ , (b)  $\bar{\epsilon}_{xx} = 0.025$ , (c)  $\bar{\epsilon}_{xx} = 0.037$ , and (d)  $\bar{\epsilon}_{xx} = 0.044$  and right at the predicted failure. The deformation bands with  $\epsilon_{\max}$  higher than 0.14 are colored gray.**

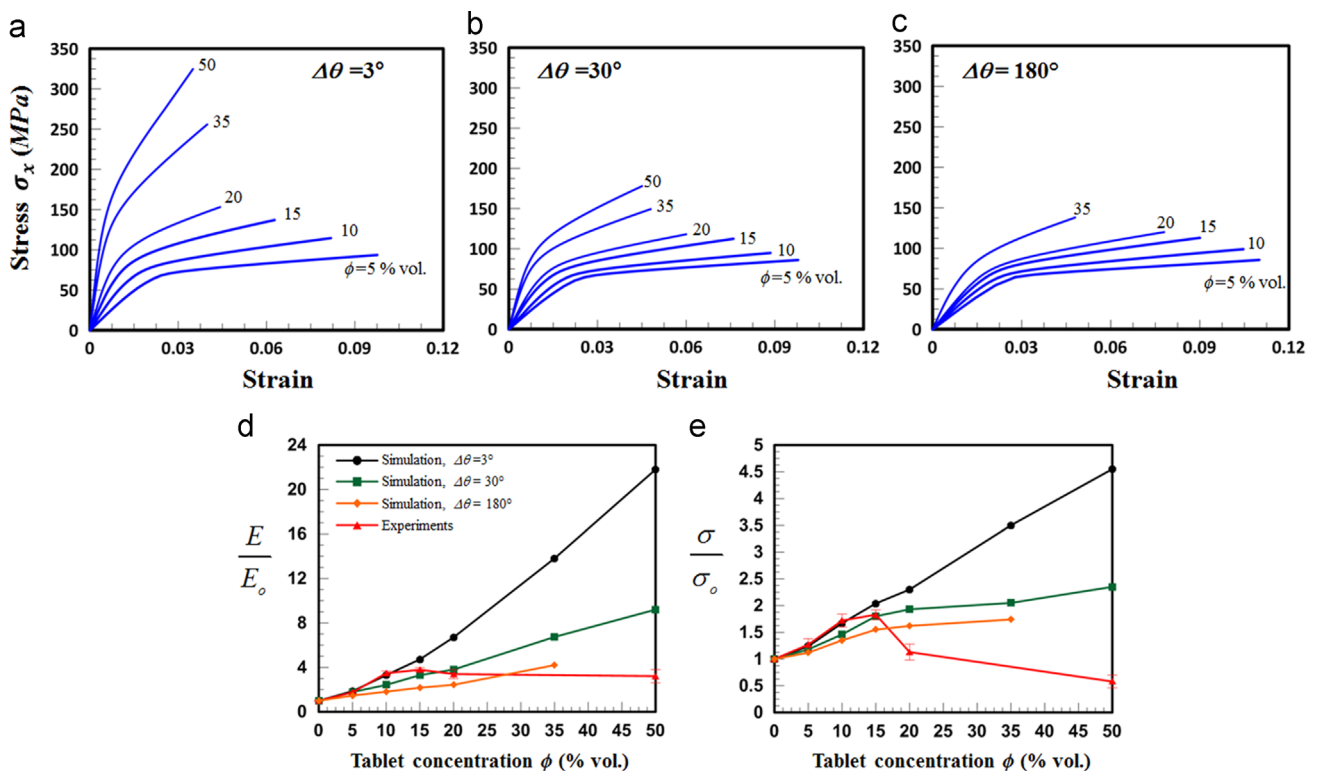


**Fig. 9 – The simulation tensile stress–strain curves for different tablet concentrations  $\phi=0, 5, 10, 15, 20, 35, 50$  vol%, when (a)  $\Delta\theta=3^\circ$ , (b)  $\Delta\theta=30^\circ$ , and (c)  $\Delta\theta=180^\circ$ . (d and e) Simulation and experimental results for (d) modulus and (e) strength. Both are normalized with the properties of the pure chitosan.**

than 0.14 propagated across the RVE, i.e. a dominant deformation band developed across the entire cross section of the material. The value of 0.14 was chosen because it is the actual maximum tensile strain of chitosan in the experiments (Fig. 4b). The size of the RVE was increased until the behavior of the material was unaffected by further increase in size, and we found that RVE with  $L=100$  tablet thicknesses was sufficiently large to statistically capture the mechanical properties of the material.

Fig. 9 shows a series of simulated tensile stress strain curves at  $\Delta\theta=3^\circ$  (high tablet alignment, Fig. 9a),  $\Delta\theta=30^\circ$

(Fig. 9b), and  $\Delta\theta=180^\circ$  (low tablet alignment, Fig. 9c). For each of these distributions of angles, the simulated stress strain curves corresponding to different tablet concentrations ( $\phi=0, 5, 10, 15, 20, 35, 50$  vol%) are shown. The results show that the modulus and strength increase with tablet volume fraction. This improvement is pronounced when the tablets are well aligned with the direction of loading ( $\Delta\theta=3^\circ$ ), but less significant when the tablets are more randomly oriented ( $\Delta\theta=180^\circ$ ) (note that the results for tablet concentration of  $\phi=50$  vol% and tablet misalignment factor  $\Delta\theta=180^\circ$  are

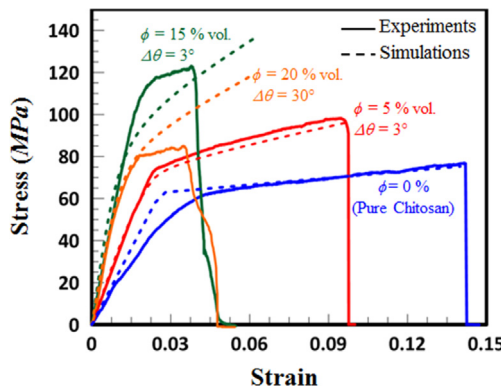


**Fig. 10 – Comparison between the experimental and simulation tensile stress-strain curves.**

absent because it was not possible to generate an RVE based on these parameters without colliding the tablets).

The simulation results for modulus (Fig. 9d) and strength (Fig. 9e) as functions of tablet concentration and for different degrees of misalignment are also plotted against the experimental data for comparison. These properties are normalized by the properties of chitosan (elastic modulus  $E_0$ , ultimate tensile strength  $\sigma_0$ ) in order to show the effect of incorporating hard tablets within a soft matrix. At low tablet volume fractions, the experimental data is consistent with the models with high tablet alignment ( $\Delta\theta=3^\circ$ ). At higher concentrations, the experiment deviates toward the models with lower levels of alignment ( $\Delta\theta=30^\circ$ ,  $180^\circ$ ). Model and experiments can therefore be reconciled by taking into account the increasing misalignment of the tablets when the concentration of the tablets is increased. The experimental observations discussed above also showed that the alignment of the tablets decreases when their concentration increases. It is therefore conceivable that the properties of the film decrease at high tablet concentration because of the increasing misalignment of the tablets.

Fig. 10 shows a set of experimental stress strain curves together with the predictions from models. A reasonable agreement between models and experiments is possible if one considers that the misalignment increases with volume concentration (from  $\Delta\theta=3^\circ$  for  $\phi=5$ , 15% to

$\Delta\theta=30^\circ$  for  $\phi=20\%$ ). The RVE based finite element models can therefore properly capture the sub-optimal performance of staggered composition when the tablets are misaligned. At tablet concentrations higher than 35 vol%, all the models including the extreme case of  $\Delta\theta=180^\circ$  over predict the experimental data for modulus, strength and energy absorption. This discrepancy indicates that other structural defects such as empty spaces, voids or tablet clustering which were all observed at appearing at larger concentrations (empty spaces, voids or tablet clustering) have a pronounced effect on mechanical performance. The discrepancies between model and experiments might also stem from certain assumptions of the model such as 2D plain strain condition, perfect bonding between the two phases, and uniformly shaped and sized tablet. In the actual experiments, the tablets are three-dimensional, their shape is irregular, their size covers a large distribution and delamination between the

tablet and polymer phases might be a dominant failure mode. In the future, the model discussed in this study will be expanded to a 3D model which considers the effect of tablet clustering for example by generating a randomized high tablet density areas (or volumes) within the RVE, effect of voids by generating empty spaces, and effect of delamination for instance by using cohesive elements at the interface between the two phases (Rabiei et al., 2010).

## 5. Conclusions

The design, optimization and fabrication of bio-inspired staggered composites at the micro and nano-scales has been the focus of intense research for more than two decades. It is now possible to fabricate nacre-like materials with high structural fidelity and high mechanical performance using methods such as freeze casting, but these methods are difficult to scale up. Other simpler methods based on mixing allow for the production of large volume of materials, but their performance decreases beyond 15–20% of tablet concentration. In this study we developed a simple, fast and versatile technique based on doctor blading to fabricate nacre-like composite films of micron-sized alumina tablets and chitosan. Doctor blading proved to be a rapid and easy method to achieve nacre-like materials with structure comparable to material obtained with more lengthy and complex methods. Consistent with previous observation, we found that the mechanical properties increased significantly with increasing tablet content, but only up to 15% after which all properties decreased. In order to explain this undesirable trend, fracture surface micrographs of the composite films were analyzed. We found that, despite the well-aligned arrangement of the tablets in all the composites resulting in a nacre-like morphology, microstructural defects such as tablet misalignment and clustering were only present at high tablet contents. Representative element models of simulated microstructures were able to accurately predict the stiffness, strength, energy absorption and strain at failure of staggered composites. The results also showed that the modulus and strength of the material can degrade significantly at higher tablet concentrations if the level of tablet misalignment increases in the composite. The results therefore provide novel insights into the structure property relations and the reasons behind the degradation of mechanical properties in staggered composite. The lack of this proper control explains why most of the studies on the development of bio-inspired materials at nano/micro scales are currently limited to low contents of tablets, where misalignment does not significantly affect the mechanical properties (Bonderer et al., 2008; Podsiadlo et al., 2007; Walther et al., 2010). For this reason, bottom-up chemical self-assembly (Mirkhalaf et al., 2015; Yeom et al., 2014), freeze casting (Bouville et al., 2014) and top down techniques such as laser engraving (Mirkhalaf and Barthelat, 2015) and lithographic techniques (Chen et al., 2007) show large potential in fabrication of bio-inspired hard materials in near future.

## Acknowledgments

This work was supported by the Fonds de Recherche du Québec – Nature et Technologies and by the Natural Sciences and Engineering Research Council of Canada. MM was partially supported by a McGill Engineering Doctoral Award. The authors are grateful to Professor Chris Barrett for the TGA analyses and to Professor Luc Mongeau for the VIC-2D software.

## REFERENCES

- Almqvist, N., Thomson, N.H., Smith, B.L., Stucky, G.D., Morse, D.E., Hansma, P.K., 1999. Methods for fabricating and characterizing a new generation of biomimetic materials. *Mater. Sci. Eng. C* 7, 37–43.
- Andres, C.M., Kotov, N.A., 2010. Inkjet deposition of layer-by-layer assembled films. *J. Am. Chem. Soc.* 132, 14496–14502.
- Ashby, M., Gibson, L., Wegst, U., Olive, R., 1995. The mechanical properties of natural materials. I. Material property charts. *Proc. R. Soc. Lond. Ser. A: Math. Phys. Sci.* 450, 123–140.
- Barbosa, S.E., Kenny, J.M., 2000. Processing of short-fiber reinforced polypropylene. I. Influence of processing conditions on the morphology of extruded filaments. *Polym. Eng. Sci.* 40, 11–22.
- Barthelat, F., 2007. Biomimetics for next generation materials. *Philos. Trans. R. Soc. B* 365, 2907–2919.
- Barthelat, F., 2014. Designing nacre-like materials for simultaneous stiffness, strength and toughness: optimum materials, composition, microstructure and size. *J. Mech. Phys. Solids* 73, 22–37.
- Barthelat, F., Mirkhalaf, M., 2013. The quest for stiff, strong and tough hybrid materials: an exhaustive exploration. *J. R. Soc. Interface* 10, 20130711.
- Barthelat, F., Rabiei, R., 2011. Toughness amplification in natural composites. *J. Mech. Phys. Solids* 59, 829–840.
- Barthelat, F., Tang, H., Zavattieri, P.D., Li, C.M., Espinosa, H.D., 2007. On the mechanics of mother-of-pearl: a key feature in the material hierarchical structure. *J. Mech. Phys. Solids* 55, 306–337.
- Barthelat, F., Zhu, D., 2011. A novel biomimetic material duplicating the structure and mechanics of natural nacre. *J. Mater. Res.* 26, 1203–1215.
- Bekah, S., Rabiei, R., Barthelat, F., 2011. Structure, scaling, and performance of natural micro- and nanocomposites. *BioNanoScience* 1, 1–9.
- Bonderer, L.J., Studart, A.R., Gauckler, L.J., 2008. Bioinspired design and assembly of platelet reinforced polymer films. *Science* 319, 1069–1073.
- Bouville, F., Maire, E., Meille, S., Van de Moortèle, B., Stevenson, A.J., Deville, S., 2014. Strong, tough and stiff bioinspired ceramics from brittle constituents. *Nat. Mater.* 13, 508–514.
- Buehler, M.J., Keten, S., Ackbarow, T., 2008. Theoretical and computational hierarchical nanomechanics of protein materials: deformation and fracture. *Prog. Mater. Sci.* 53, 1101–1241.
- Chen, L., Ballarini, R., Kahn, H., Heuer, A., 2007. Bioinspired micro-composite structure. *J. Mater. Res.* 22, 124–131.
- Clegg, W.J., Kendall, K., Alford, N.M., Button, T.W., Birchall, J.D., 1990. A simple way to make tough ceramics. *Nature* 347, 455–457.
- Currey, J., 1977. Mechanical properties of mother of pearl in tension. *Proc. R. Soc. Lond. Ser. B: Biol. Sci.* 196, 443–463.
- Currey, J., Taylor, J., 1974. The mechanical behaviour of some molluscan hard tissues. *J. Zool.* 173, 395–406.
- Das, P., Schipmann, S., Malho, J.-M., Zhu, B., Klemradt, U., Walther, A., 2013. Facile access to large-scale, self-assembled, nacre-inspired, high-performance materials with tunable nanoscale periodicities. *ACS Appl. Mater. Interfaces* 5, 3738–3747.
- Deville, S., Saiz, E., Nalla, R.K., Tomsia, A.P., 2006. Freezing as a path to build complex composites. *Science* 311, 515–518.
- Dimas, L.S., Bratzel, G.H., Eylon, I., Buehler, M.J., 2013. Tough composites inspired by mineralized natural materials: computation, 3D printing, and testing. *Adv. Funct. Mater.* 23, 4629–4638.
- Erb, R.M., Libanori, R., Rothfuchs, N., Studart, A.R., 2012. Composites reinforced in three dimensions by using low-magnetic fields. *Science* 335, 199–204.
- Espinosa, H.D., Rim, J.E., Barthelat, F., Buehler, M.J., 2009. Merger of structure and material in nacre and bone – perspectives on de novo biomimetic materials. *Prog. Mater. Sci.* 54, 1059–1100.
- Fratzl, P., 2003. Cellulose and collagen: from fibres to tissues. *Curr. Opin. Colloid Interface Sci.* 8, 32–39.
- Gao, H., Ji, B., Jäger, I.L., Arzt, E., Fratzl, P., 2003. Materials become insensitive to flaws at nanoscale: lessons from nature. *Proc. Natl. Acad. Sci. U.S.A.* 100, 5597–5600.
- Glavinchevski, B., Piggott, M., 1973. Steel disc reinforced polycarbonate. *J. Mater. Sci.* 8, 1373–1382.
- Guo, X., Gao, H., 2006. Bio-inspired Material Design and Optimization. Springer, Netherlands, 439–453.
- Guo, Z., Pereira, T., Choi, O., Wang, Y., Hahn, H.T., 2006. Surface functionalized alumina nanoparticle filled polymeric nanocomposites with enhanced mechanical properties. *J. Mater. Chem.* 16, 2800–2808.
- He, J.L., Li, W.Z., Li, H.D., 1997. Simulation of nacre with TiN/Pt multilayers and a study of their hardness. *J. Mater. Res.* 12, 3140–3145.
- Hunger, P.M., Donius, A.E., Wegst, U.G., 2012. Platelets self-assemble into porous nacre during freeze casting. *J. Mech. Behav. Biomed. Mater.* 19, 87–93.
- Jackson, A.P., Vincent, J.F.V., Turner, R.M., 1988. The mechanical design of nacre. *Proc. R. Soc. B* 234, 415–440.
- Jager, I., Fratzl, P., 2000. Mineralized collagen fibrils: a mechanical model with a staggered arrangement of mineral particles. *Biophys. J.* 79, 1737–1746.
- Joseph, K., Thomas, S., Pavithran, C., Brahmakumar, M., 1993. Tensile properties of short sisal fiber-reinforced polyethylene composites. *J. Appl. Polym. Sci.* 47, 1731–1739.
- Katti, D.R., Katti, K.S., Sopp, J.M., Sarikaya, M., 2001. 3D finite element modeling of mechanical response in nacre-based hybrid nanocomposites. *Comput. Theor. Polym. Sci.* 11, 397–404.
- Knudsen, F., 1962. Effect of porosity on Young's modulus of alumina. *J. Am. Ceram. Soc.* 45, 94–95.
- Kotha, S.P., Li, Y., Guzelsu, N., 2001. Micromechanical model of nacre tested in tension. *J. Mater. Sci.* 36, 2001–2007.
- Ma, P.C., Kim, J.-K., Tang, B.Z., 2007. Effects of silane functionalization on the properties of carbon nanotube/epoxy nanocomposites. *Compos. Sci. Technol.* 67, 2965–2972.
- Mayer, G., 2006. New classes of tough composite materials – lessons from natural rigid biological systems. *Mater. Sci. Eng. C* 26, 1261–1268.
- Meyers, M.A., Chen, P.Y., Lin, A.Y.M., Seki, Y., 2008. Biological materials: structure and mechanical properties. *Prog. Mater. Sci.* 53, 1–206.
- Mirkhalaf, M., Barrett, C.J., Barthelat, F., 2015. Self-assembly of microscopic tablets within polymeric thin films: a possible pathway towards new hybrid materials. *RSC Adv.* 5, 4780–4787.
- Mirkhalaf, M., Barthelat, F., 2014. The Effect of Dilution Natural and Bio-inspired Staggered Composites, Mechanics of

- Biological Systems and Materials, 4. Springer, United States of America (US), 83–91.
- Mirkhalaf, M., Barthelat, F., 2015. A laser-engraved glass duplicating the structure, mechanics and performance of natural nacre. *Bioinspir. Biomim.* 10, 026005.
- Mirkhalaf, M., Dastjerdi, A.K., Barthelat, F., 2014. Overcoming the brittleness of glass through bio-inspiration and micro-architecture. *Nat. Commun.* 5, 3166.
- Mirkhalaf, M., Deju, Z., Barthelat, F., 2013. Biomimetic hard materials. In: Lakhtakia, A., Martin-Palma, R.J. (Eds.), *Engineered Biomimicry*. Elsevier Inc., New York.
- Munch, E., Launey, M.E., Alsem, D.H., Saiz, E., Tomsia, A.P., Ritchie, R.O., 2008. Tough, bio-inspired hybrid materials. *Science* 322, 1516–1520.
- Ortiz, C., Boyce, M.C., 2008. Bioinspired structural materials. *Science* 319, 1053–1054.
- Podsiadlo, P., Kaushik, A.K., Arruda, E.M., Waas, A.M., Shim, B.S., Xu, J., Nandivada, H., Pumplin, B.G., Lahann, J., Ramamoorthy, A., Kotov, N.A., 2007. Ultrastrong and stiff layered polymer nanocomposites. *Science* 318, 80–83.
- Qian, H., Greenhalgh, E.S., Shaffer, M.S., Bismarck, A., 2010. Carbon nanotube-based hierarchical composites: a review. *J. Mater. Chem.* 20, 4751–4762.
- Rabiei, R., Bekah, S., Barthelat, F., 2010. Failure mode transition in nacre and bone-like materials. *Acta Biomater.* 6, 4081–4089.
- Rintoul, M.D., Torquato, S., 1997. Reconstruction of the structure of dispersions. *J. Colloid Interface Sci.* 186, 467–476.
- Ritchie, R.O., 2011. The conflicts between strength and toughness. *Nat. Mater.* 10, 817–822.
- Tang, Z., Kotov, N.A., Magonov, S., Ozturk, B., 2003. Nanostructured artificial nacre. *Nat. Mater.* 2, 413–418.
- Walther, A., Bjurhager, I., Malho, J.M., Pere, J., Ruokolainen, J., Berglund, L.A., Ikkala, O., 2010. Large-area, lightweight and thick biomimetic composites with superior material properties via fast, economic, and green pathways. *Nano Lett.* 10, 2742–2748.
- Wang, J., Cheng, Q., Lin, L., Chen, L., Jiang, L., 2013. Understanding the relationship of performance with nanofiller content in the biomimetic layered nanocomposites. *Nanoscale* 5, 6356–6362.
- Wang, R.Z., Suo, Z., Evans, A.G., Yao, N., Aksay, I.A., 2001. Deformation mechanisms in nacre. *J. Mater. Res.* 16, 2485–2493.
- Wise, S.W., 1970. Microarchitecture and deposition of gastropod nacre. *Science* 167, 1486–1488.
- Yao, H.B., Tan, Z.H., Fang, H.Y., Yu, S.H., 2010. Artificial nacre-like bionanocomposite films from the self-assembly of chitosan-montmorillonite hybrid building blocks. *Angew. Chem. – Int. Ed.* 49, 10127–10131.
- Yeom, J., Yeom, B., Chan, H., Smith, K.W., Dominguez-Medina, S., Bahng, J.H., Zhao, G., Chang, W.-S., Chang, S.-J., Chuvalin, A., 2014. Chiral templating of self-assembling nanostructures by circularly polarized light. *Nat. Mater.* 14, 66–72.